SANDIA REPORT
SAND2007-5872
Unlimited Release
Printed September, 2007

Testing of Constitutive Models in LAME

William M. Scherzinger
Daniel C. Hammerand

Prepared by
Sandia National Laboratories
Albuquerque, New Mexico 87185 and Livermore, California 94550

Sandia is a multiprogram laboratory operated by Sandia Corporation,
a Lockheed Martin Company, for the United States Department of Energy's
National Nuclear Security Administration under Contract DE-AC04-94AL85000.

Issued by Sandia National Laboratories, operated for the United States Department of Energy by Sandia Corporation.

Available to DOE and DOE contractors from
U.S. Department of Energy
Office of Scientific and Technical Information
P.O. Box 62
Oak Ridge, TN 37831

Telephone: (865) 576-8401
Facsimile: (865) 576-5728
E-Mail: reports@adonis.osti.gov
Online ordering: http://www.osti.gov/bridge

Available to the public from
U.S. Department of Commerce
National Technical Information Service
5285 Port Royal Rd.
Springfield, VA 22161

Telephone: (800) 553-6847
Facsimile: (703) 605-6900
E-Mail: orders@ntis.fedworld.gov
Online order: http://www.ntis.gov/help/ordermethods.asp?loc=7-4-0#online

SAND2007-5872
Unlimited Release
Printed September 2007

Testing of Constitutive Models in LAME

William M. Scherzinger and Daniel C. Hammerand
Solid Mechanics – 1524
Sandia National Laboratories
P.O. Box 5800
Albuquerque, New Mexico 87185-MS0372

Abstract

Constitutive models for computational solid mechanics codes are in LAME – the Library of Advanced Materials for Engineering. These models describe complex material behavior and are used in our finite deformation solid mechanics codes. To ensure the correct implementation of these models, regression tests have been created for constitutive models in LAME. A selection of these tests is documented here.

ACKNOWLEDGMENTS

The authors would like to acknowledge the help of a number of people at Sandia National Laboratories. The Adagio and Presto code development teams, including Arne Gullerud, Kendall Pierson, Jason Hales, Nathan Crane and Bill Gilmartin have been especially helpful in the development of LAME and the interface between Strumento and LAME. The SNTools team, especially Mark Hamilton and Kevin Brown, have helped with code management issues. A number of constitutive model developers, including Bob Chambers, Mike Neilsen and Shane Schumacher, have given very useful feedback on the design of LAME. Finally, analysts that have been willing to use LAME, Jeff Gruda, Matthew Neidigk and Frank Dempsey, have also helped guide its design.

CONTENTS

FIGURES

TABLES

1. INTRODUCTION

Constitutive models are an important part of any solid mechanics code. If an analysis code is meant to provide accurate results, the constitutive models that describe the material behavior need to be implemented correctly. Ensuring the correct implementation of constitutive models is the goal of a testing procedure that is used with the Library of Advanced Materials for Engineering (LAME) (see [1] and [2]).

A test suite for constitutive models can serve three purposes. First, the test problems provide the constitutive model developer a means to test the model implementation. This is an activity that is always done by any responsible constitutive model developer. Retaining the test problem in a repository where the problem can be run periodically is an excellent means of ensuring that the model continues to behave correctly. A second purpose of a test suite for constitutive models is that it gives application code developers confidence that the constitutive models work correctly. This is extremely important since any analyst that uses an application code for an engineering analysis will associate a constitutive model in LAME with the application code, not LAME. Therefore, ensuring the correct implementation of constitutive models is essential for application code teams. A third purpose of a constitutive model test suite is that it provides analysts with example problems that they can look at to understand the behavior of a specific model. Since the choice of a constitutive model, and the properties that are used in that model, have an enormous effect on the results of an analysis, providing problems that highlight the behavior of various constitutive models to the engineer can be of great benefit.

LAME is currently implemented in the Sierra based solid mechanics codes Adagio [3] and Presto [4]. The constitutive models in LAME are available in both codes. Due to the nature of a transient dynamics code – e.g. Presto – it is difficult to test a constitutive model due to inertia effects that show up in the solution. Therefore the testing of constitutive models is primarily done in Adagio. All of the test problems detailed in this report are run in Adagio.

It is the goal of the constitutive model test suite to provide a useful service for the constitutive model developer, application code developer and engineer that uses the application code. Due to the conflicting needs and tight time constraints on solid mechanics code development, no requirements exist for implementing test problems for constitutive models. Model developers are strongly encouraged to provide test problems and document those problems, but given the choice of having a model without a test problem or no model at all, certain requirements must be kept loose. A flexible code development environment, especially with regards to research and development in constitutive modeling, is essential to the success of such an environment.

This report provides documentation of a number of tests for the constitutive models in LAME. Each section documents a separate test with a brief description of the model, the test problem and the results. This report is meant to be updated periodically as more test problems are created and put into the test suite.

2. GENERAL CONSTITUTIVE MODEL TESTING

The means of testing constitutive models is something that cannot be defined in general. Each model will have unique capabilities that need to be tested. What should be tested is any capability that the constitutive model has. What is tested, in reality, are those capabilities deemed to be important by the constitutive model developer.

It is not the purpose of this document to determine exactly what tests a constitutive model developer should run to check their model. Rather, this document will provide a number of examples of tests that are run for many of the models in LAME.

2.1 Mesh for Verification Tests

This mesh that is used for most of the verification tests is the same mesh that is used for the patch test in Adagio and Presto – a cube with seven elements. The mesh is shown in Figure 1. The elements in this mesh are not parallelepipeds, so this mesh is a good test of linear consistency for the elements, hence its usefulness as a patch test. If the constitutive model is implemented correctly, a test with this mesh can be run where, if a linear displacement field is placed on the eight exterior nodes of the cube, not only is the correct stress found, but that stress is the same for every element.

The patch-test mesh has eight exterior nodes that are used to define boundary conditions. The

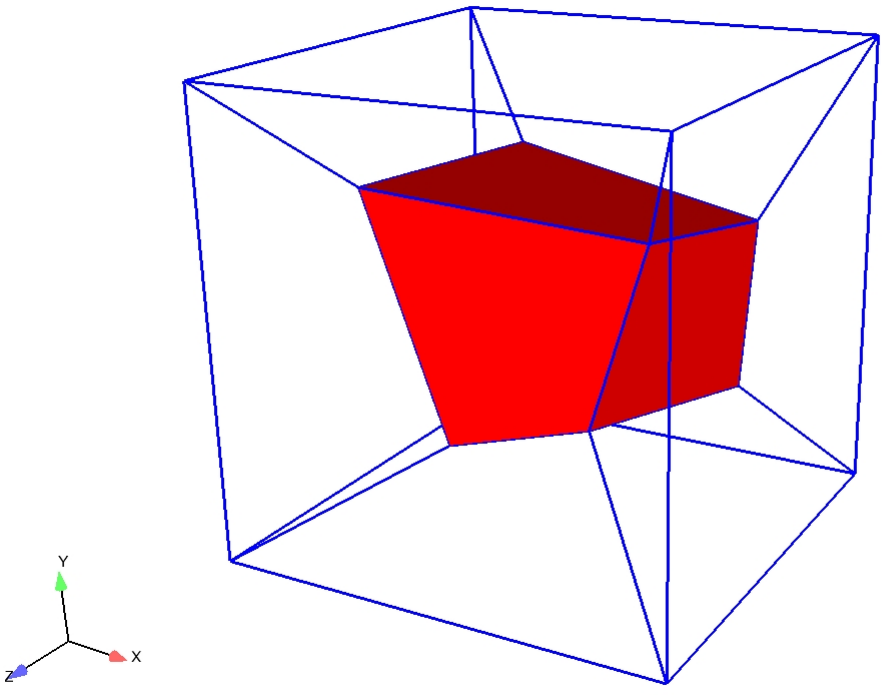

Figure 1: The seven element patch test mesh used for constitutive model verification. The center element is element number 1.

boundary conditions can have prescribed displacements or tractions. The boundary conditions can be along coordinate axes or any set of user defined axes. With this capability, verification tests can be created with a number of different boundary conditions: prescribed displacement, prescribed traction or mixed boundary conditions. A simpler mesh – a single element – can also be used. A test of this type run is Adagio would mimic exactly a point simulator. Finally, it should be noted that with either mesh, a uniform strain field is the expected result of any applied boundary conditions. Therefore, hourglass control should have no effect on the solution.

3. MATERIAL MODEL TESTS

A number of material models in LAME have regression tests in Adagio and Presto that test the implementation and capabilities of the models. This section documents these tests and provides examples for tests that can be run for different constitutive models. Constitutive modelers are encouraged to develop test problems for any model that they implement in LAME. The documentation in this section provides examples for the types of tests that they can develop for their models. The application code developers for Adagio and Presto use these tests in their nightly regression test suite to ensure that no code changes have occurred that might affect functionality. Any application code that uses LAME is encouraged to develop the same tests for their application code. Analysts can also use the tests that are documented here to understand what to expect from the constitutive models that they are using in their analysis.

The test problems in this section represent only some of the test problems that are in the regression test suites for LAME. There are currently over 80 regression tests for constitutive models that are in LAME. The test suites are a part of the Adagio and Presto regression test suites. As more problems are documented and/or created they will be added to this report.

3.1 Elastic Test

The simplest test is the regression test that is run for the elastic model. This test is a uniaxial stress test. The test uses the patch-test mesh of a unit cube shown in Figure 1.

A uniaxial stress is prescribed using displacement control in the x direction and traction-free boundary conditions in the y and z directions. The prescribed displacement is such that the displacement of the $-x$ face is zero and the displacement of the $+x$ face has a maximum of 0.005 in. and a minimum of -0.005 in. Since the initial geometry is of a unit cube, i.e. a 1 in. cube, the maximum and minimum strains are

$$\begin{aligned} \varepsilon_{\max} &= \ln\left(1.005\right) = 4.9875\times10^{-3} \\ \varepsilon_{\min} &= \ln\left(0.995\right) = -5.0125\times10^{-3} \end{aligned} \quad . \tag{1}$$

The prescribed displacement/strain as a function of time is given in Table 1.

Table 1. Displacement boundary condition for elastic test

time	displacement	axial strain
0.00 s	0.000 in	0.0000
0.25 s	0.005 in	4.9875×10^{-3}
0.75 s	-0.005 in	-5.0125×10^{-3}
1.00 s	0.000 in	0.0000

The material constants for the elastic model that are used in this problem are shown in Table 2.

Table 2. Material properties for elastic test

property	value
YOUNGS MODULUS	10×10^{6} psi
POISSONS RATIO	0.25

Given a uniaxial strain problem on a unit cube with zero lateral tractions, the stress calculated using an elastic model is

$$\sigma_{xx} = E\varepsilon_{xx} = E\ln\left(1+u_x\right) , \tag{2}$$

where E is the Young's modulus and u is the prescribed displacement in the x direction. Using the values for the prescribed displacements in Table 1 and the material properties in Table 2, the maximum and minimum axial stresses are 49.875×10^{3} psi and -50.125×10^{3} psi respectively.

Since the lateral surfaces are traction free they are free to contract. The displacement of the lateral surface is

$$u_y = u_z = \frac{1}{\left(1+u_x\right)^{\nu}} - 1 \ . \tag{3}$$

Using the prescribed displacements in Table 1, the minimum and maximum lateral displacements are -1.2461×10^{-3} in. and 1.2539×10^{-3} in. respectively.

3.1.1 Results for Elastic Test

The results for the elastic test match exactly the expected results presented above. A plot of the six stress components is shown in Figure 2. The only non-zero stress component is σ_{xx}. The other five components are zero.

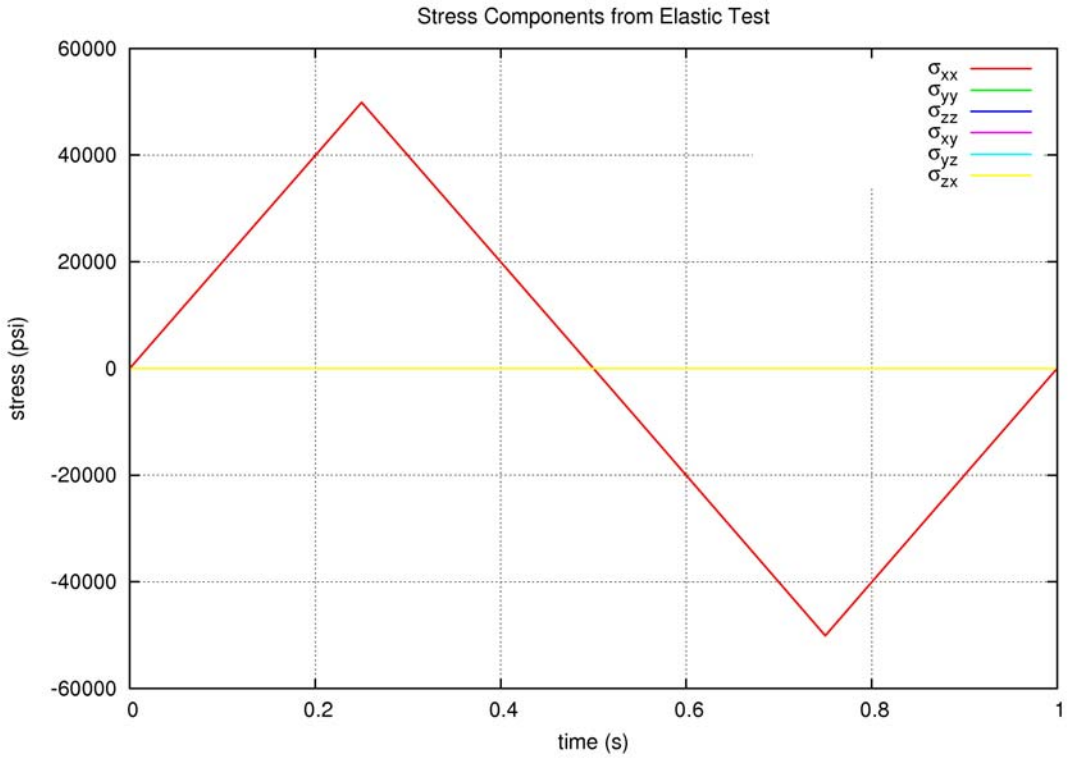

Figure 2: Results for the stress components of element number 1 in the elastic test problem.

3.2 Thermoelastic Test

The verification test for the thermoelastic model is designed to test the model under a combination of mechanical and thermal loading. The constitutive model has temperature dependent material properties, i.e. a temperature dependent Young's modulus and a temperature dependent Poisson's ratio. The test problem does not use thermal strains since thermal strains are currently handled outside of LAME. The mesh for the problem is the mesh shown in Figure 1.

Table 3. Room temperature material properties for thermoelastic test

property	value
YOUNGS MODULUS	1×10^{3} psi
POISSONS RATIO	0.25

The test problem has two stages: a mechanical one and a thermal one. The test problem lasts two

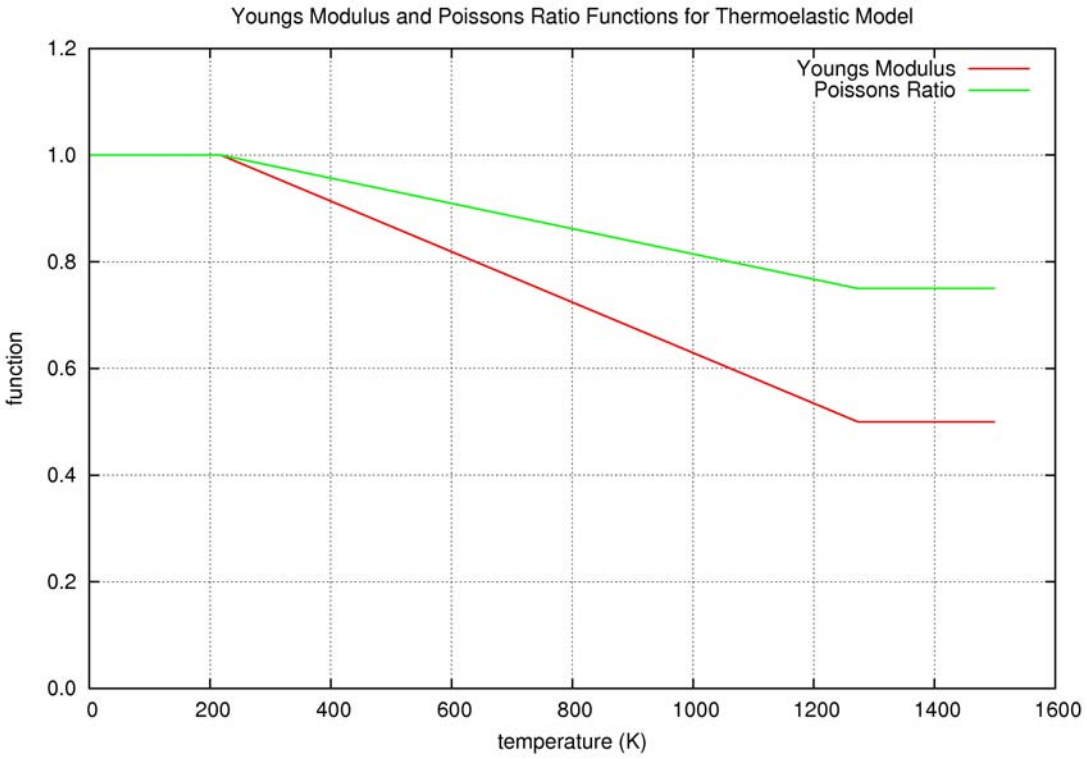

Figure 3: Normalized functions for the Young's modulus and Poisson's ratio as a function of temperature.

seconds. From zero seconds to one second the material is stretched isothermally from its initial configuration to an axial strain of 4.9875×10^{-3}. For stage two the axial strain is held fixed while the temperature increases from room temperature to $1{,}000^{\circ}$C. This increase in temperature causes a change in the elastic properties that will result in a change in the axial stress. It should be noted that the values used for this test problem are completely fictitious. Furthermore, since the test is run with Adagio, a quasi-static code, the solution to the problem is independent of the loading rate.

The reference temperature constitutive properties for the thermoelastic model used in the test problem are shown in Table 3. For temperatures other than the reference temperature, two functions describe how the constitutive properties change with temperature. These functions are shown in Figure 3.

Since the problem is uniaxial stress, the axial stress in the problem is simply

$$\sigma_{xx} = E\left(T\right)\varepsilon_{xx} \ . \tag{4}$$

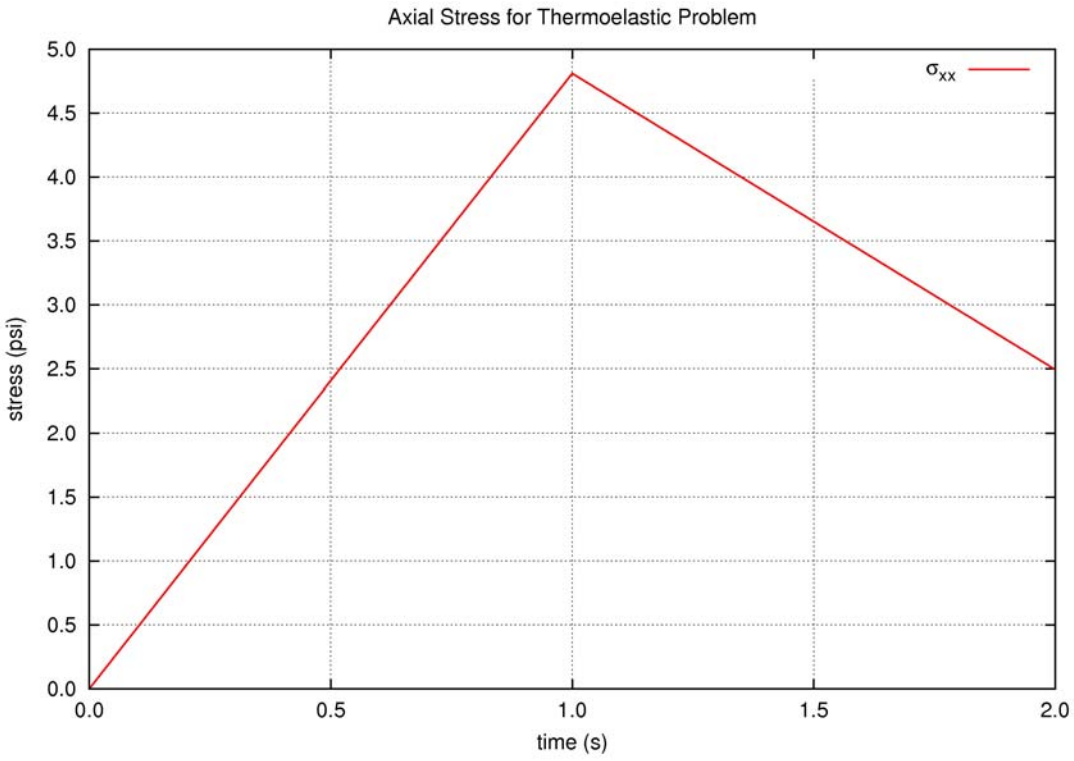

Figure 4: The axial stress in the thermoelastic test as a function of time. Up until 1 second the stress is mechanical, from 1 second to 2 seconds the stress decreases due to the reduction in the elastic modulus from an increase in temperature.

At room temperature (the reference temperature) the normalized function is 1.0. At $1,000^\circ$ C the normalized function is 0.5. Therefore, at room temperature the Young's modulus is 1×10^3 psi, while at $1,000^\circ$ C the Young's modulus is 500 psi. Given that the axial strain is 4.9875×10^{-3}, the axial stress at room temperature will be 4.9875 psi. After the temperature rises to $1,000^\circ$ C the axial stress will drop to 2.4938 psi.

In a similar manner, the lateral strain can be calculated. From the normalized curves for the Poisson's ratio, the Poisson's ratio at $1,000^\circ$ C will be 0.1875. From this we can calculate the lateral strain at room temperature, with an axial strain of 4.9875×10^{-3}, will be -1.2469×10^{-3}, while at $1,000^\circ$ C the lateral strain will be -0.9352×10^{-3}. These strains will result in lateral displacements of -1.2461×10^{-3} in and -0.9347×10^{-3} in.

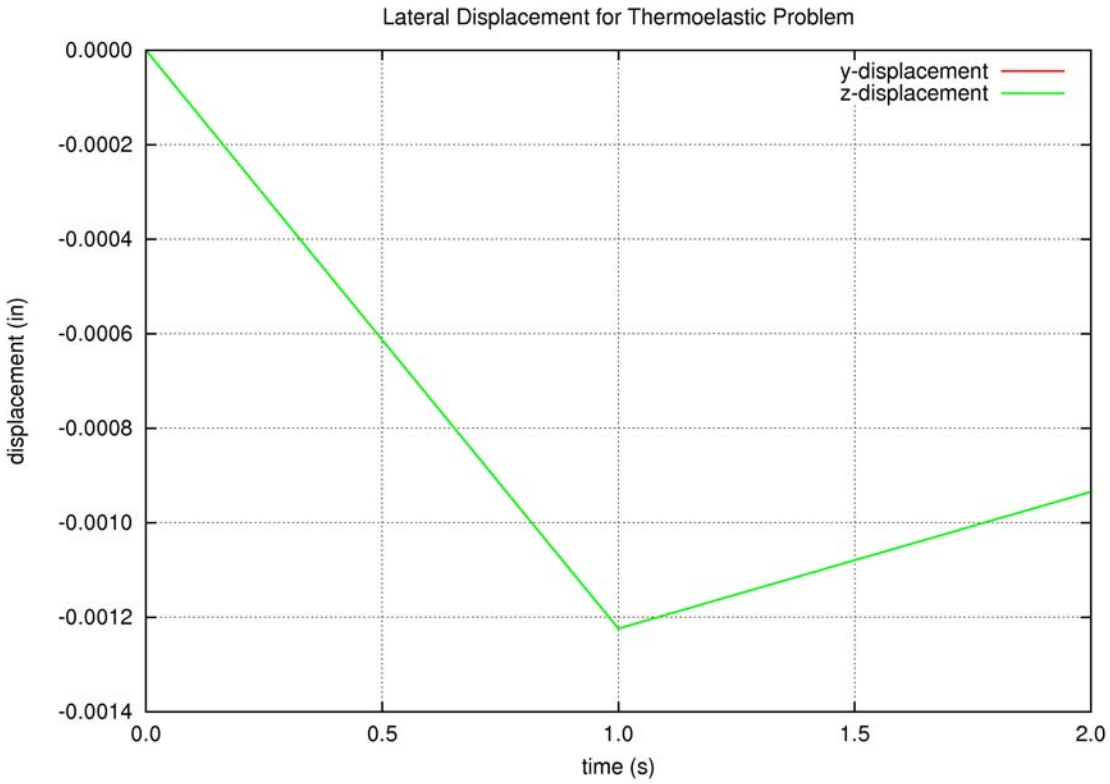

Figure 5: The lateral displacements in the thermoelastic test as a function of time. Up until 1 second the loading is mechanical, from 1 second to 2 seconds the lateral displacement decreases due to the reduction in the Poisson's ratio from an increase in temperature.

3.2.1 Results for Thermoelastic Test

The results for the thermoelastic test match the expected results exactly. The axial stress as a function of time is shown in Figure 4. Here the stress up to 1 second is from strictly mechanical loading at the reference temperature (i.e. room temperature). At 1 second the mechanical loading, through displacement control, stops and the temperature rises to $1,000^{\circ}$ C. This causes a drop in the elastic modulus and a corresponding decrease in the stress. By the end of the analysis the elastic modulus and the stress are both one-half of their values at room temperature.

The results showing the lateral displacement as a function of time are shown in Figure 5. Once again these results match perfectly the expected results due to the reduction in the Poisson's ratio.

3.3 Elastic-Plastic Test

The verification test for the elastic-plastic, linear hardening model is similar to the elastic test in that it models uniaxial stress with a prescribed displacement. The elastic-plastic linear hardening model is described in [5] and [6].

The test is different from the elastic test in that is has three unit cubes rather than one. The three separate cubes allow us to test the elastic-plastic model with isotropic hardening, kinematic hardening and combined hardening all in one test.

Uniaxial stress is prescribed in all three cubes using displacement control in the x direction and traction-free boundary conditions in the y and z directions. The prescribed displacement is such that the displacements of the $-x$ faces of the cubes are zero and the displacements of the $+x$ faces have a maximum of 0.005 in. and a minimum of -0.005 in. Since the initial geometry is of a unit cube, i.e. a 1 in. cube, the maximum and minimum strains in each cube are

$$\begin{aligned} \varepsilon_{\max} &= \ln\left(1.005\right) = 4.9875\times10^{-3} \\ \varepsilon_{\min} &= \ln\left(0.995\right) = -5.0125\times10^{-3} \end{aligned} \quad . \tag{5}$$

The prescribed displacement/strain as a function of time is given in Table 4.

Table 4. Displacement boundary condition for elastic-plastic test

time	displacement	axial strain
0.00 s	0.000 in	0.0000
0.25 s	0.005 in	4.9875×10^{-3}
0.75 s	-0.005 in	-5.0125×10^{-3}
1.00 s	0.000 in	0.0000

The material constants for the isotropic hardening problem are shown in Table 5. The material constants for the kinematic hardening problem are shown in Table 6. The material constants for the combined hardening problem are shown in Table 7.

The hardening behavior – isotropic, kinematic or combined – determines how the yield surface either grows or moves in stress space to accommodate loading outside of the yield surface. A difference in the results will be seen if loading is reversed, as it is in this verification problem. For the initial loading, from 0.0 to 0.25 s, the results are the same for isotropic, kinematic and combined hardening. At 0.25 s the loading is reversed and the material unloads. The material state is now inside of the yield surface and will eventually hit the opposite side of the yield surface. Whether the yield surface is growing in size (isotropic hardening) and/or moving in stress space (kinematic hardening) will determine when the stress state reaches the yield surface and begins to show plastic deformation. A pure kinematic hardening model ($\beta = 0.0$) will

Table 5. Material properties for elastic-plastic test with isotropic hardening

property	value
YOUNGS MODULUS	10×10^{6} psi
POISSONS RATIO	0.25
YIELD STRESS	10×10^{3} psi
HARDENING MODULUS	100×10^{3} psi
BETA	1.0

Table 6. Material properties for elastic-plastic test with kinematic hardening

property	value
YOUNGS MODULUS	10×10^{6} psi
POISSONS RATIO	0.25
YIELD STRESS	10×10^{3} psi
HARDENING MODULUS	100×10^{3} psi
BETA	0.0

Table 7. Material properties for elastic-plastic test with combined hardening

property	value
YOUNGS MODULUS	10×10^{6} psi
POISSONS RATIO	0.25
YIELD STRESS	10×10^{3} psi
HARDENING MODULUS	100×10^{3} psi
BETA	0.5

predict plastic re-loading first, a combined model ($0.0 < \beta < 1.0$) will predict plastic re-loading second, and an isotropic model ($\beta = 1.0$) will predict plastic re-loading last.

At 0.75 s, the material has resumed plastic loading for all three models, and the loading is reversed again. Once again the material state is now inside the yield surface until it hits the yield surface on the other side of the elastic domain. The same behavior is observed in this reversal as was seen in the fist reversal at 0.25 s – plastic loading of the kinematic hardening model, followed by the combined hardening model, followed by the isotropic hardening model.

The response for all three problems starts as an elastic response followed by yielding of the material once the uniaxial stress reaches the yield stress. The response after yield is the elastic-plastic response which continues until un-loading at $t = 0.25\,\text{s}$. Once the loading is reversed, the response is elastic. The subsequent yield after load reversal will depend on the hardening law. The material with the kinematic hardening law, where the yield surface moves in stress space, will yield first, followed by the material with the combined hardening law, where the yield surface both moves and grows, followed by the material with the isotropic hardening law, where the yield surface is stationary but grows.

3.3.1 Results for Elastic-Plastic Test

The results for the elastic-plastic test are exactly what is expected. The axial stress from the test is shown in Figure 6 for all three models – isotropic, kinematic and combined hardening – along with the exact solutions for the isotropic and kinematic hardening cases. The behavior is the same until the material state hits the yield surface after the first unloading. After this the kinematic hardening model has the lowest stress value (in absolute value) and the isotropic hardening model has the highest stress value. The combined hardening model lies between the other two.

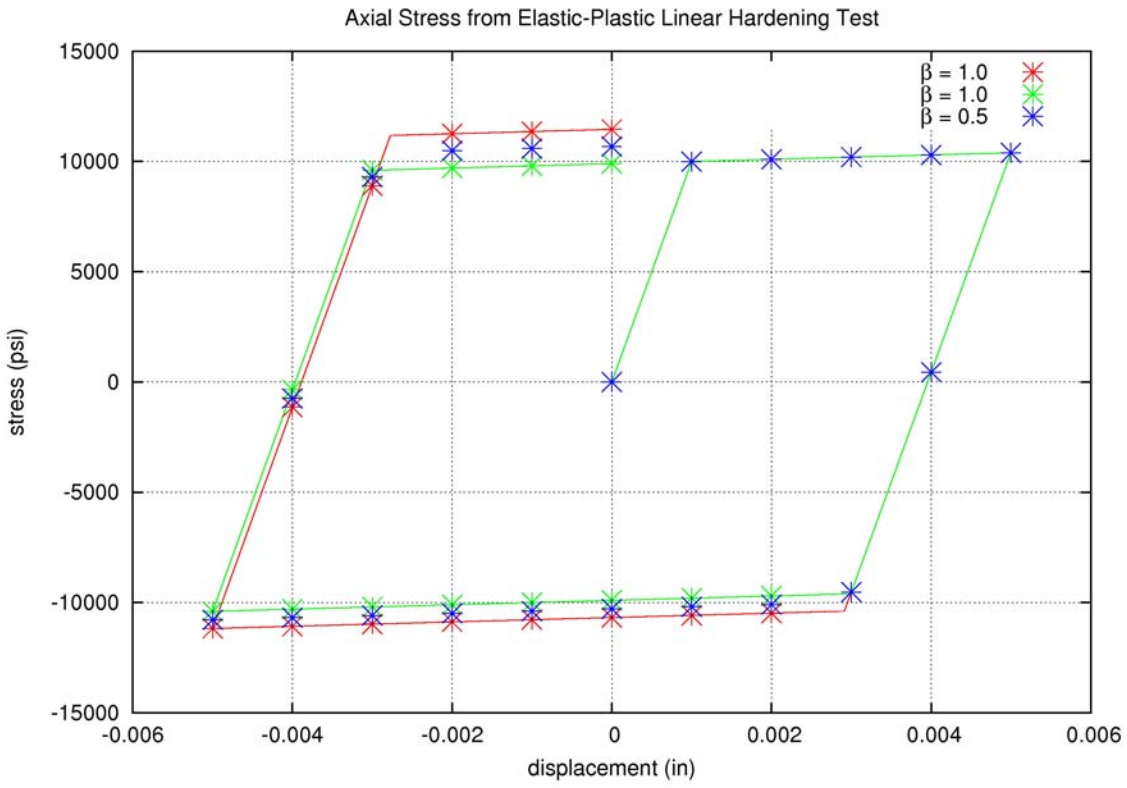

Figure 6: The axial stress components from the elastic-plastic linear hardening test. Results are shown for isotropic hardening ($\beta = 1.0$), kinematic hardening ($\beta = 0.0$) and a combination of isotropic and kinematic hardening ($\beta = 0.5$). The exact results for isotropic and kinematic hardening are given by the red and green lines respectively.

3.4 Elastic-Plastic Power Law Hardening Test

The verification test for the elastic-plastic power law hardening test is similar to the test for the elastic-plastic linear hardening test. The elastic-plastic power law hardening model is described in [5] and [7]. The mesh for the problem is shown in Figure 1.

A uniaxial stress is prescribed using displacement control in the x direction and traction-free boundary conditions in the y and z directions. The prescribed displacement is such that the displacement of the $-x$ face is zero and the displacement of the $+x$ face has a maximum of 0.005 in. and a minimum of -0.005 in. Since the initial geometry is of a unit cube, i.e. a 1 in. cube, the maximum and minimum strains are

$$\begin{aligned} \varepsilon_{\max} &= \ln\left(1.005\right) = 4.9875\times10^{-3} \\ \varepsilon_{\min} &= \ln\left(0.995\right) = -5.0125\times10^{-3} \end{aligned} \quad . \tag{6}$$

The prescribed displacement/strain as a function of time is given in Table 8.

Table 8. Displacement boundary condition for elastic-plastic power law hardening test

time	displacement	axial strain
0.00 s	0.000 in	0.0000
0.25 s	0.005 in	4.9875×10^{-3}
0.75 s	-0.005 in	-5.0125×10^{-3}
1.00 s	0.000 in	0.0000

The material constants for the elastic-plastic power law hardening model that are used in this problem are shown in Table 9.

Table 9. Material properties for elastic-plastic power law hardening test

property	value
YOUNGS MODULUS	1×10^{3} psi
POISSONS RATIO	0.25
YIELD STRESS	1.0 psi
HARDENING CONSTANT	1.0 psi
HARDENING EXPONENT	0.25
LUDERS STRAIN	0.002

The response of the material in this problem is initially elastic. After yield, the material is perfectly plastic exhibiting a Lüders band. Once the equivalent plastic strain surpasses the Lüders strain, the material starts to harden with a power law relationship. At 0.25 seconds the

loading is reversed and elastic unloading occurs. Once the state hits the yield surface, the material continues to harden until loading is reversed again at 0.75 seconds. Elastic unloading occurs again, followed by hardening once the state hits the yield surface.

3.4.1 Results for Elastic-Plastic Power Law Hardening Test

The results for the elastic-plastic power law hardening test are shown in Figure 7. The plot shows the axial stress (which is equal to the von Mises stress) versus the end displacement for the unit cube. The Lüders band is obvious in the test results, followed by the power law hardening. Load reversal is seen at an end displacement of 0.005 in. This load reversal results in elastic unloading, followed by continued hardening. Another load reversal occurs at an end displacement of -0.005 in. Again this load reversal results in elastic unloading, followed by continued hardening. These results are expected in the power law hardening model; an exact solution was not calculated for this test.

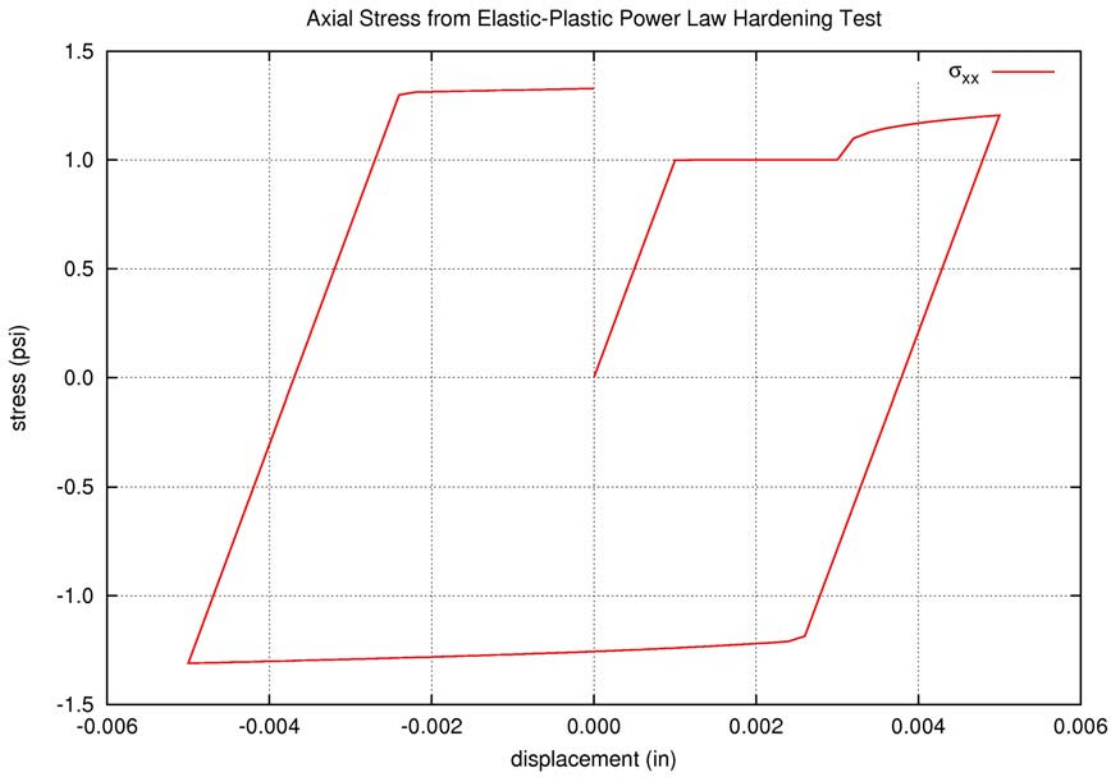

Figure 7: The axial stress component from the elastic-plastic power law hardening test showing axial stress versus end displacement.

3.5 Thermoelastic-Plastic Power Law Hardening Test

The thermoelastic-plastic power law hardening test uses the THERMO_EP_POWER model. This model is a power law hardening model with an underlying thermoelastic elasticity model. In addition to having the Young's modulus and the Poisson's ratio as functions of temperature, the yield stress is also a function of temperature. One other feature of this model that is not present in the power law hardening elastic-plastic model is the ability to model kinematic hardening.

Table 10. Room temperature material properties for thermoelastic-plastic power law hardening test with isotropic hardening

property	value
YOUNGS MODULUS	1×10^3 psi
POISSONS RATIO	0.25
YIELD STRESS	1.0 psi
HARDENING CONSTANT	1.0 psi
HARDENING EXPONENT	0.25
LUDERS STRAIN	0.002
BETA	1.0

Table 11. Room temperature material properties for thermoelastic-plastic power law hardening test with kinematic hardening

property	value
YOUNGS MODULUS	1×10^3 psi
POISSONS RATIO	0.25
YIELD STRESS	1.0 psi
HARDENING CONSTANT	1.0 psi
HARDENING EXPONENT	0.25
LUDERS STRAIN	0.002
BETA	0.0

Table 12. Material properties for thermoelastic-plastic power law hardening test with combined hardening

property	value
YOUNGS MODULUS	1×10^3 psi
POISSONS RATIO	0.25
YIELD STRESS	1.0 psi
HARDENING CONSTANT	1.0 psi
HARDENING EXPONENT	0.25
LUDERS STRAIN	0.002
BETA	0.5

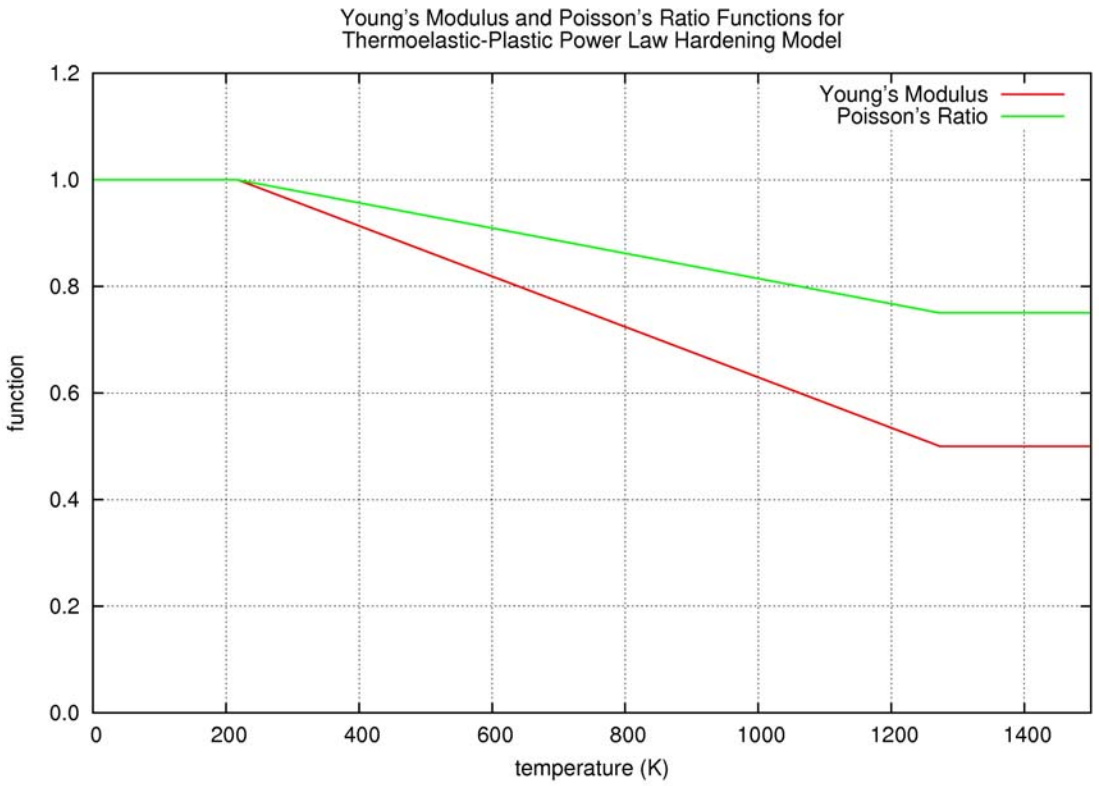

Figure 8: Normalized functions for the Young's modulus and Poisson's ratio as a function of temperature for the thermoelastic-plastic power law hardening model.

The test problem is similar to the elastic-plastic linear hardening model due to the need to test the isotropic, kinematic and combined hardening aspects of the model. In this test there are three element blocks, one for each type of hardening. The material properties are shown in Table 10, Table 11 and Table 12.

The thermal loading in this test involves a temperature increase from 20° C to 1000° C. The increase in temperature of the material will affect the elastic properties and the yield stress.

3.5.1 Results for Thermoelastic-Plastic Power Law Hardening Test

Since the underlying elastic model and the yield stress vary as a function of temperature, the results from the test are difficult to interpret. However, it is expected that the results will show that the three models will track each other until the yield surface is engaged after the initial unloading. This is the same behavior that was observed in the elastic-plastic linear hardening test. After re-engaging the yield surface, the kinematic hardening model will have the lowest stress in absolute value, followed by the combined hardening model and then the isotropic hardening model.

The results are shown in Figure 9. These results show the expected behavior with load reversals, engaging the yield surface at different locations and a general decrease in the radius of the yield surface. An analytical solution was not generated for this test problem.

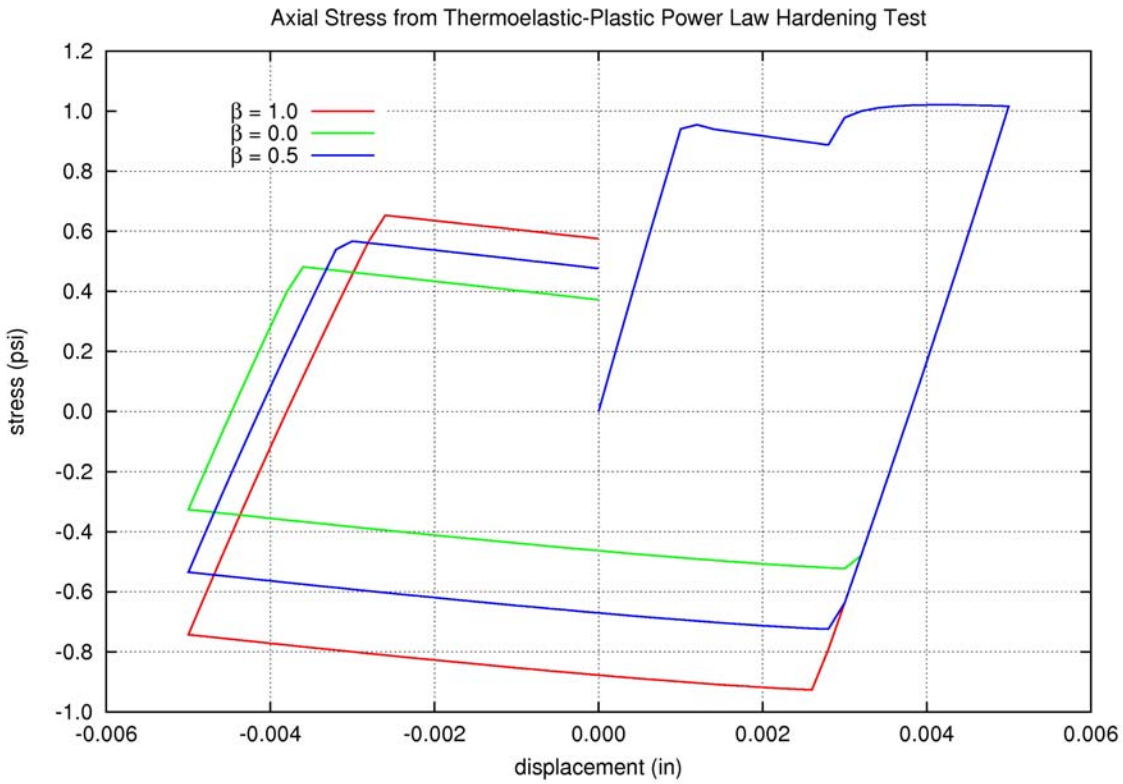

Figure 9: The axial stress components from the thermoelastic-plastic power law hardening test. Results are shown for isotropic hardening ($\beta = 1.0$), kinematic hardening ($\beta = 0.0$) and a combination of isotropic and kinematic hardening ($\beta = 0.5$).

3.6 Power Law Creep Test

The verification test for the power law creep test involves the uniaxial loading of a block through displacement control, followed by stress relaxation. The power law creep model is a secondary creep model that is described in [5]. The mesh for the problem is shown in Figure 1.

The power law creep model describes the evolution of the creep strain, ε_c, as a function of the von Mises stress, $\bar{\sigma}$

$$\dot{\varepsilon}_c = A\bar{\sigma}^m \exp(-B) \ , \tag{7}$$

where A is the creep constant, m is the creep exponent and B is the thermal constant. The material properties used in the power law creep test are given in Table 13.

Table 13. Material properties for the power law creep test

property	value
YOUNGS MODULUS	90.68×10^3 kPa
POISSONS RATIO	0.39
CREEP CONSTANT	5.116×10^{-5}
CREEP EXPONENT	4.51
THERMAL CONSTANT	29.5

The test problem is an axial displacement control problem. The end displacement ramps up to 0.01 over 100 seconds and is held constant until 1,000 seconds. While the strain is fixed, the inelastic strain, or creep strain, evolves according to (7). The evolution of the creep strain causes a relaxation in the axial stress.

The problem can be formulated as an ordinary differential equation. Using an additive decomposition for the strain rate

$$\dot{\varepsilon} = \dot{\varepsilon}_e + \dot{\varepsilon}_c \ , \tag{8}$$

where $\dot{\varepsilon}_e$ is the elastic strain rate,and the fact that the stress depends only on the elastic strain, we obtain the following non-linear ODE for the axial stress

$$\dot{\sigma} + EAe^{-B}\sigma^m - E\dot{\varepsilon} = 0 \, . \tag{9}$$

For the initial 100 seconds the strain rate can be calculated from the uniform axial displacement

$$\dot{\varepsilon} = \dot{\lambda}/\lambda \ , \tag{10}$$

while for the final 900 seconds the strain rate is zero. The rest of the terms in (9) are constants.

3.6.1 Results for Power Law Creep Test

The results for the power law creep test are shown in Figure 10. The stress ramps up during the initial loading which is subsequently followed by stress relaxation.

An analytical solution to (9) does not exist in general; it must be solved numerically. A numerical solution to (9) can be found using, for example, a Runga-Kutta algorithm. This was done for this problem and the results in Figure 10 matched the numerical solution to the problem.

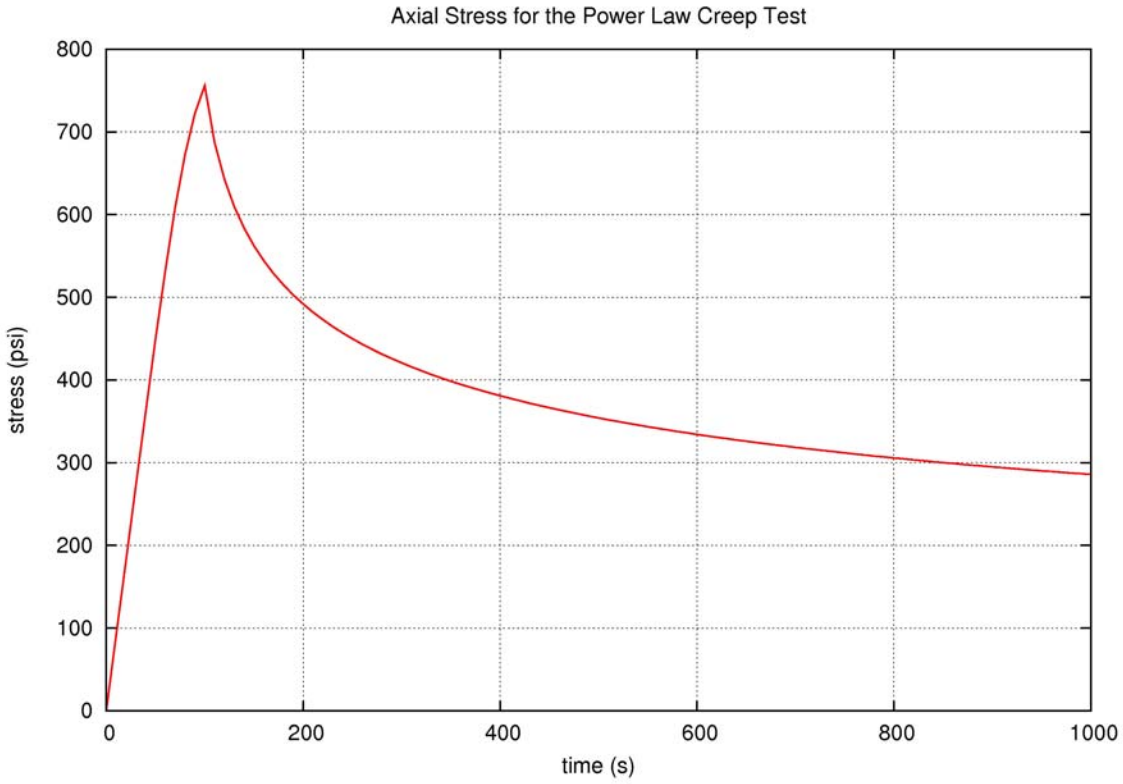

Figure 10: Axial stress from the power law creep test.

3.7 Soil and Foam Test

The soil and foam model is a versatile model that is capable of modeling geologic materials and crushable foams. The soil and foam model is described in [5], [6]and [8].

Table 14. Material properties for soil and foam test

property	value
SHEAR MODULUS	27.815×10^{9} Pa
BULK MODULUS	83.444×10^{9} Pa
A0	2.3383×10^{6} Pa
A1	2.3383
A2	0.0
PRESSURE CUTOFF	-1.0×10^{6} Pa

The test verification test problem for the soil and foam model tests a Drucker-Prager model that exhibits pressure dependence of the yield surface. The material properties used for the Drucker-Prager model are given in Table 14.

The values for A0 and A1 describe a linear relationship between the radius of the yield surface

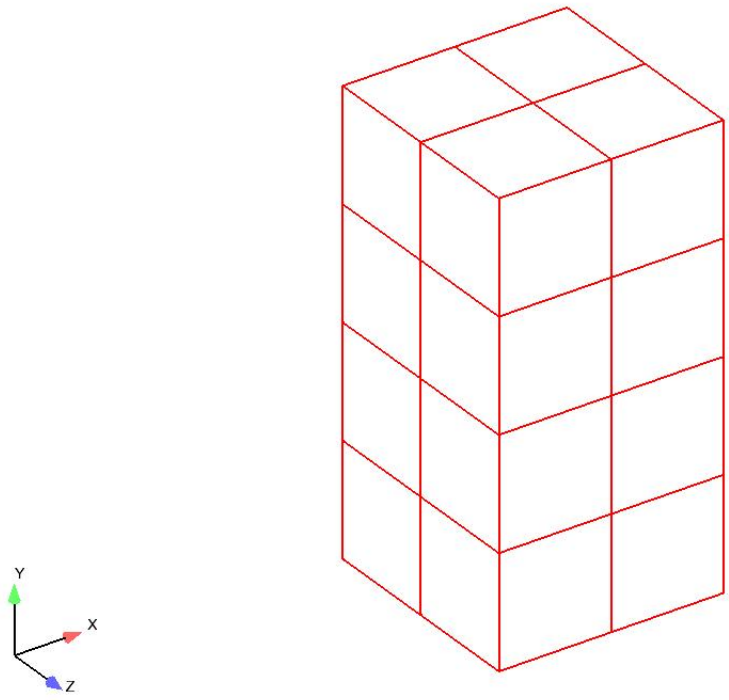

Figure 11: 16 element mesh for the soil and foam test.

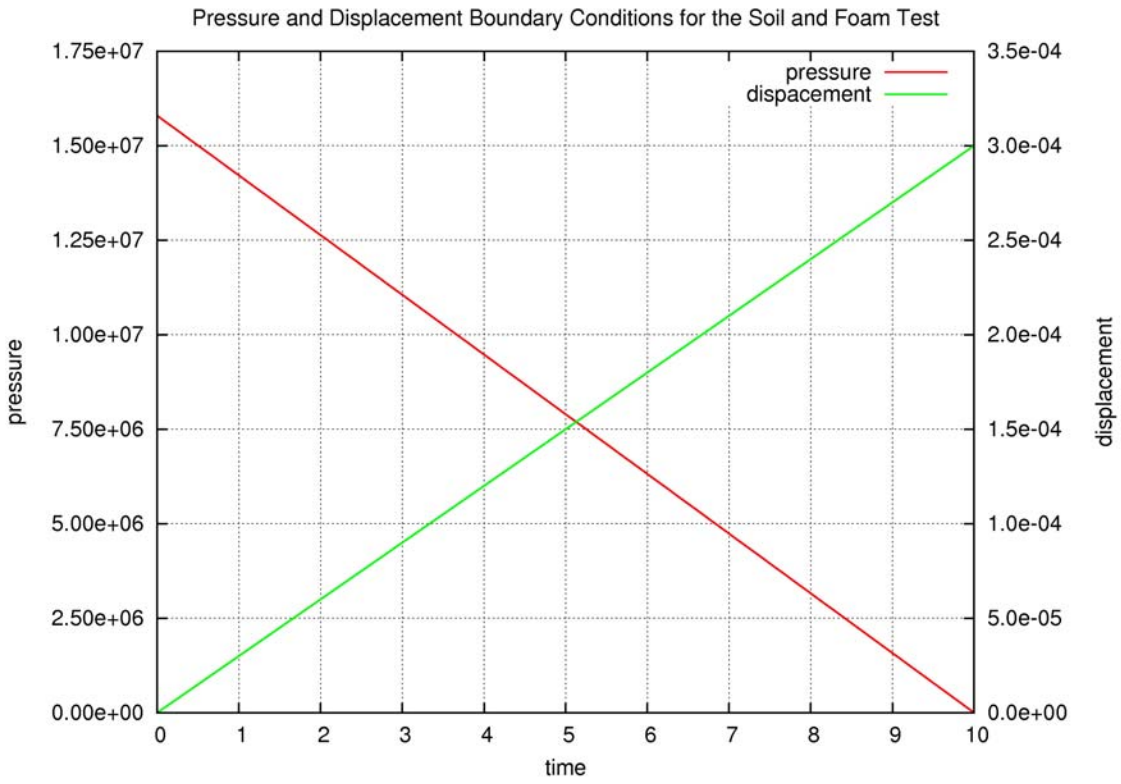

Figure 12: Boundary conditions for the soil and foam test problem.

and the pressure.

The mesh for the problem is shown in Figure 11. It is a square column that is four elements high, and two by two in the *x*-*z* plane.

The displacement boundary conditions for this problem are fixed normal to the $-x$, $-y$ and $-z$ faces of the mesh – resulting in symmetry planes on these surfaces. A pressure boundary condition is placed on the $+x$ and $+z$ faces. A prescribed displacement in the *y*-direction is placed on the $+y$ face. The time variation of the pressure and the displacement boundary conditions are shown in Figure 12. The boundary conditions will result in an initial state of biaxial stress that transitions to a state of uniaxial stress. The pressure will decrease while the effective stress will initially decrease, pass through a state of pure pressure, then increase again, intersecting the yield surface at some point.

3.7.1 Results for Soil and Foam Test

The results for the soil and foam test match the expected behavior. A plot showing the yield surface and the stress state throughout the analysis is shown in Figure 13. These results show that the material behaves exactly as expected.

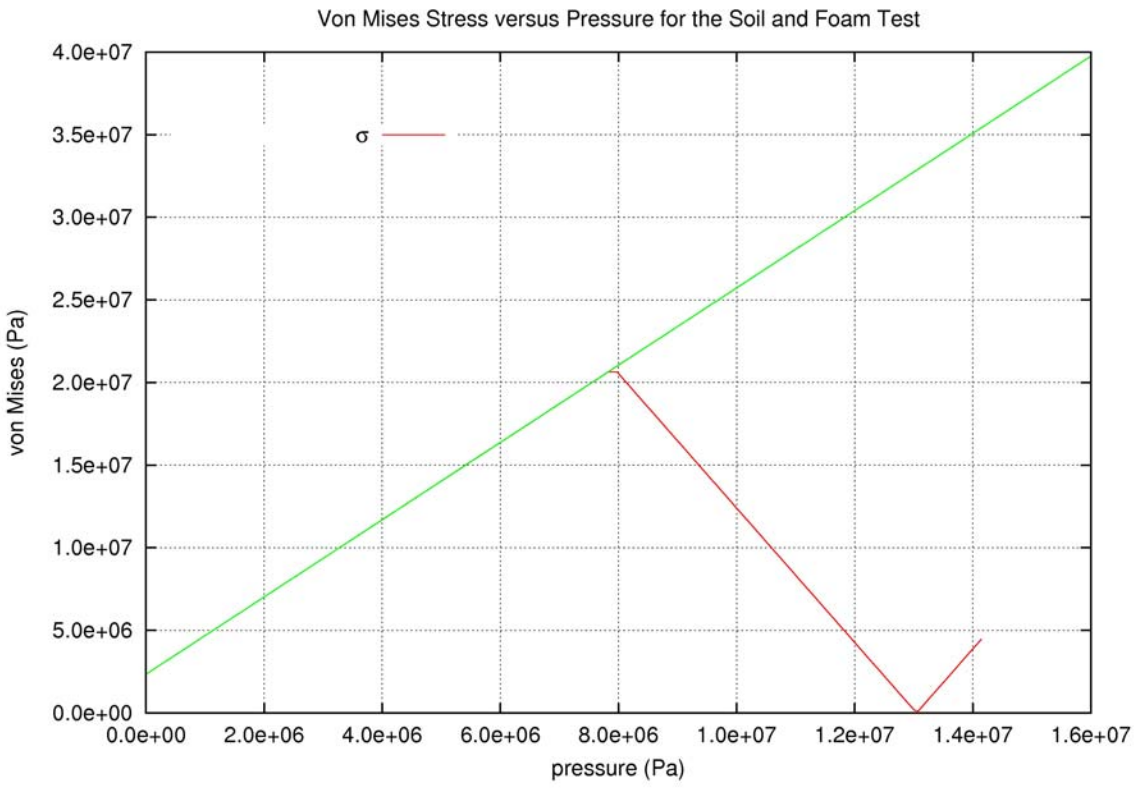

Figure 13: Results showing the von Mises stress versus the pressure for the soil and foam test using a Drucker-Prager model. The green line is the pressure dependent yield surface for the material.

3.8 Neo-Hookean Test

Two test problems are run for the neo-Hookean model: a uniaxial strain test and a simple shear test. Both of these tests are completely displacement control. As a result, the deformation and strain are known and the stress can easily be computed. The mesh for each problem is the same as the patch-test mesh in Figure 1. The constitutive model is described in [9].

The strain energy density for the neo-Hookean model is

$$W(\mathbf{C}) = \frac{1}{4}K\left[\det\mathbf{C} - \ln(\det\mathbf{C}) - 1\right] + \frac{1}{2}\mu\left(\frac{\mathrm{tr}\mathbf{C}}{\det\mathbf{C}^{1/3}} - 3\right), \tag{11}$$

where $\mathbf{C}$ is the right Cauchy-Green tensor. There are two material properties for this model, the bulk modulus, K, and the shear modulus, μ.

Table 15. Material properties for the neo-Hookean test

property	value
BULK MODULUS	0.500 MPa
SHEAR MODULUS	0.375 MPa

The second Piola-Kirchoff stress is calculated from (11)

$$S_{ij} = 2\frac{\partial W}{\partial C_{ij}}, \tag{12}$$

and the Cauchy stress is

$$\sigma_{ij} = \frac{1}{J}F_{ik}S_{kl}F_{jl}. \tag{13}$$

It is worth noting that $C_{ij} = F_{ki}F_{kj}$ and $\det\mathbf{C} = J^2$. Using (11), the second Piola-Kirchoff stress is

$$S_{ij} = \frac{1}{2}KC_{ij}^{-1}\left(J^2 - 1\right) + \mu\left(\delta_{ij} - \frac{1}{3}C_{ij}^{-1}C_{kk}\right)J^{-2/3}. \tag{14}$$

The Cauchy stress is

$$\sigma_{ij} = \frac{1}{2}K\delta_{ij}\left(J - \frac{1}{J}\right) + \mu\left(B_{ij} - \frac{1}{3}\delta_{ij}B_{kk}\right)J^{-5/3}, \tag{15}$$

where $B_{ij} = F_{ik}F_{jk}$.

For the uniaxial strain neo-Hookean test, the deformation gradient is

$$\left[F_{ij}\right]=\begin{bmatrix}\lambda & 0 & 0\\ 0 & 1 & 0\\ 0 & 0 & 1\end{bmatrix}, \tag{16}$$

which, when substituted in (15), gives

$$\begin{aligned}\sigma_{11} &= \frac{1}{2}K\left(\lambda-\frac{1}{\lambda}\right)+\frac{2}{3}\mu\left(\lambda^2-1\right)\lambda^{-5/3}\\ \sigma_{22}=\sigma_{33} &= \frac{1}{2}K\left(\lambda-\frac{1}{\lambda}\right)-\frac{1}{3}\mu\left(\lambda^2-1\right)\lambda^{-5/3}\end{aligned}. \tag{17}$$

A second test is the simple shear test. This test is also entirely displacement controlled. The deformation gradient for simple shear is

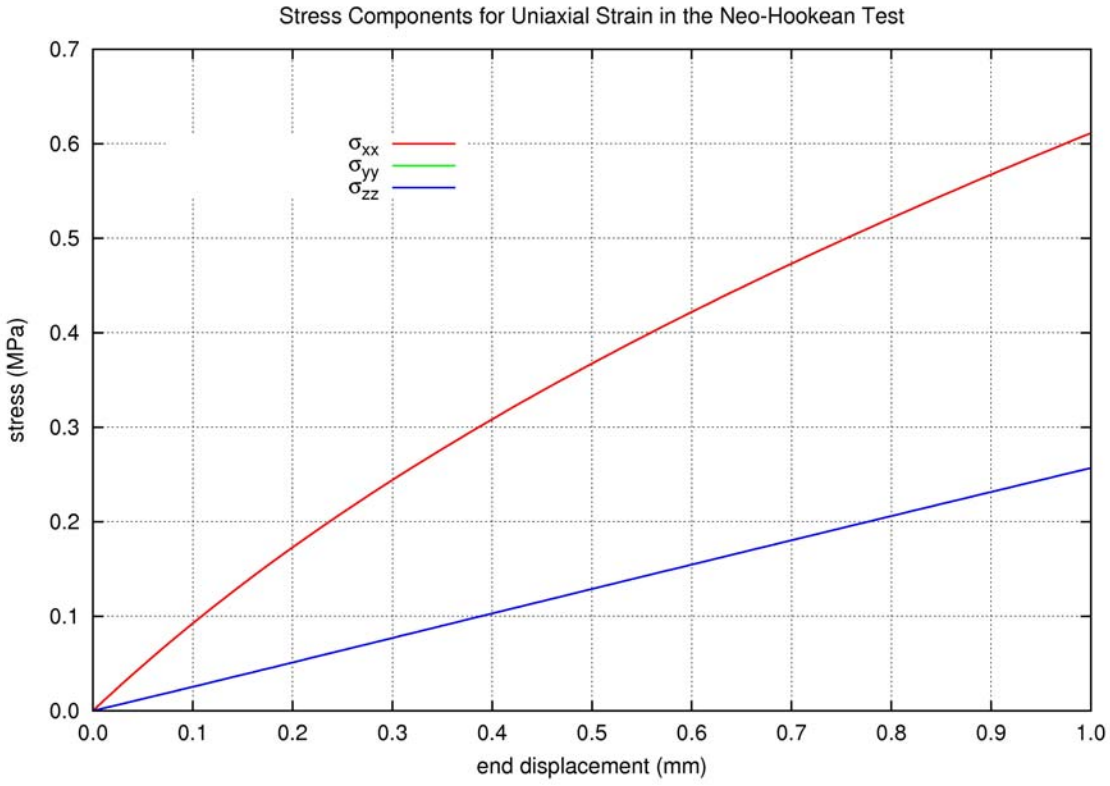

Figure 14: Stress components from the uniaxial strain neo-Hookean test.

$$\left[F_{ij}\right]=\begin{bmatrix}1 & \gamma & 0\\ 0 & 1 & 0\\ 0 & 0 & 1\end{bmatrix}. \tag{18}$$

For simple shear $J=1$ and

$$\left[B_{ij}\right]=\begin{bmatrix}1+\gamma^2 & \gamma & 0\\ \gamma & 1 & 0\\ 0 & 0 & 1\end{bmatrix}. \tag{19}$$

The trace of the left Cauchy-Green tensor is $B_{kk}=3+\gamma^2$.

The non-zero components of the Cauchy stress are

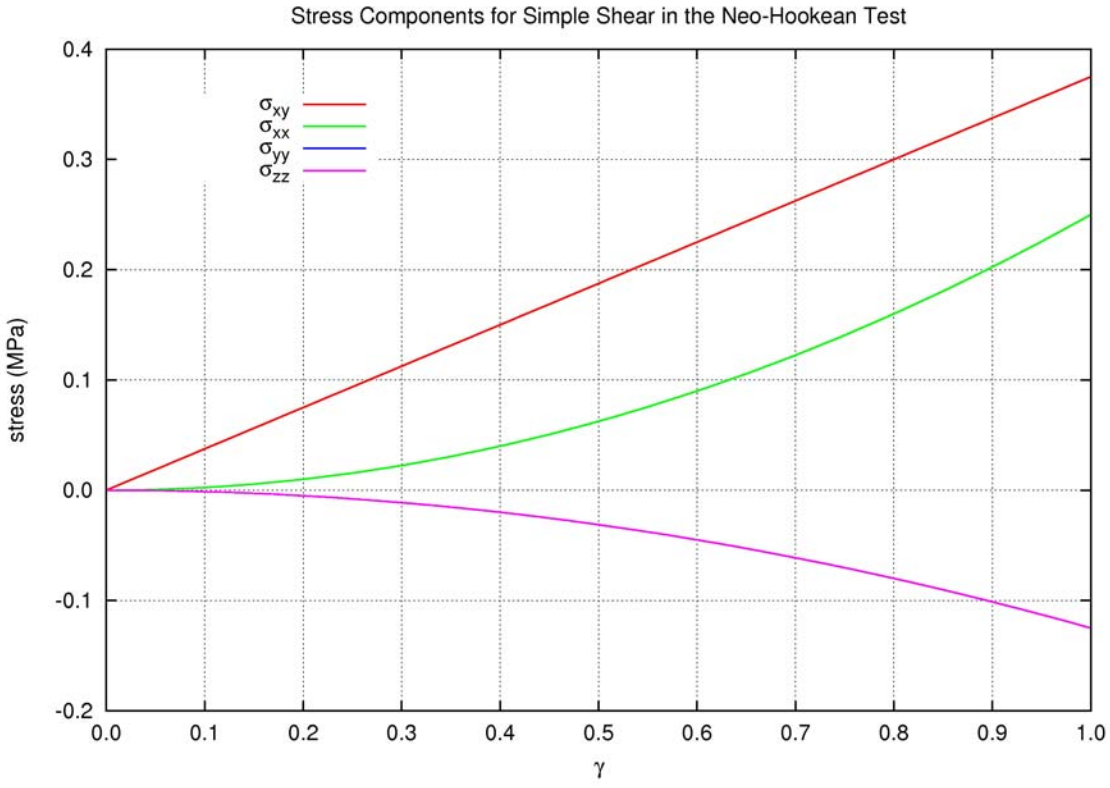

Figure 15: Stress components from the simple shear neo-Hookean test.

$$\sigma_{xy} = \mu\gamma \quad ; \quad \sigma_{xx} = \frac{2}{3}\mu\gamma^2 \quad ; \quad \sigma_{yy} = \sigma_{zz} = -\frac{1}{3}\mu\gamma^2 \ . \tag{20}$$

3.8.1 Results for Neo-Hookean Test

The results for the uniaxial test problem are shown in Figure 14 while the results for the simple shear problem are shown in Figure 15. It is easy to show that the numerical results match the analytical results in (17) and (20).

3.9 Hyperfoam Test

The hyperfoam test involves two problems: a uniaxial strain problem and a biaxial strain problem. Both problems are entirely displacement controlled. As a result, the deformation and strain are known and the stress can easily be computed. The mesh for each problem is the patch-test mesh in Figure 1.

The constitutive model is an Ogden type hyperelasticity model that is described in [10]. This model uses a series expansion for the strain energy density. The material properties used for the test problems are shown in Table 16. There are three terms used in the expansion of the strain energy density

$$W\left(\lambda_1,\lambda_2,\lambda_3\right)=\sum_{k=1}^{N}\frac{2\mu_k}{\alpha_k^2}\left[\lambda_1^{\alpha_k}+\lambda_2^{\alpha_k}+\lambda_3^{\alpha_k}-3+\frac{1}{\beta_i}\left(J^{-\alpha_k\beta_k}-1\right)\right]. \tag{21}$$

The expression for β_k can be written in terms of a Poisson's ratio, ν_k

$$\beta_k=\frac{\nu_k}{1-2\nu_k}\ . \tag{22}$$

Given the strain energy density in (21), the three principal Cauchy stresses can be written as

$$\sigma_I=\frac{\lambda_I}{J}\frac{\partial W}{\partial\lambda_I}\quad\left(\text{no sum on } I\right)\ . \tag{23}$$

Table 16. Material properties for the hyperfoam test

property	values		
SHEAR	3.74×10^6	-3.17×10^6	1.18×10^4
ALPHA	2.536	2.090	-8.807
POISSON	0.5630	0.5507	0.3662

The first test problem is uniaxial strain. For this problem the axial engineering strain is -0.6. The lateral strains are zero. For this problem the three principal stretch ratios are

$$\begin{aligned}\lambda_1&=0.4\\ \lambda_2=\lambda_3&=1.0\end{aligned}\ . \tag{24}$$

The second test problem is biaxial strain. For this problem the engineering strains are -0.6 in two coordinate directions. The third coordinate direction has a strain of zero. For this problem the three principal stretch ratios are

$$\lambda_1 = \lambda_2 = 0.4$$
$$\lambda_3 = 1.0 \quad . \tag{25}$$

For the uniaxial strain problem the principal stresses are

$$\sigma_1 = \frac{1}{\lambda}\sum_{k=1}^{3}\frac{2\mu_k}{\alpha_k}\left(\lambda^{\alpha_k} - \lambda^{-\alpha_k\beta_k}\right)$$
$$\sigma_2 = \sigma_3 = \frac{1}{\lambda}\sum_{k=1}^{3}\frac{2\mu_k}{\alpha_k}\left(1 - \lambda^{-\alpha_k\beta_k}\right) \quad . \tag{26}$$

For the biaxial strain problem the principal stresses are

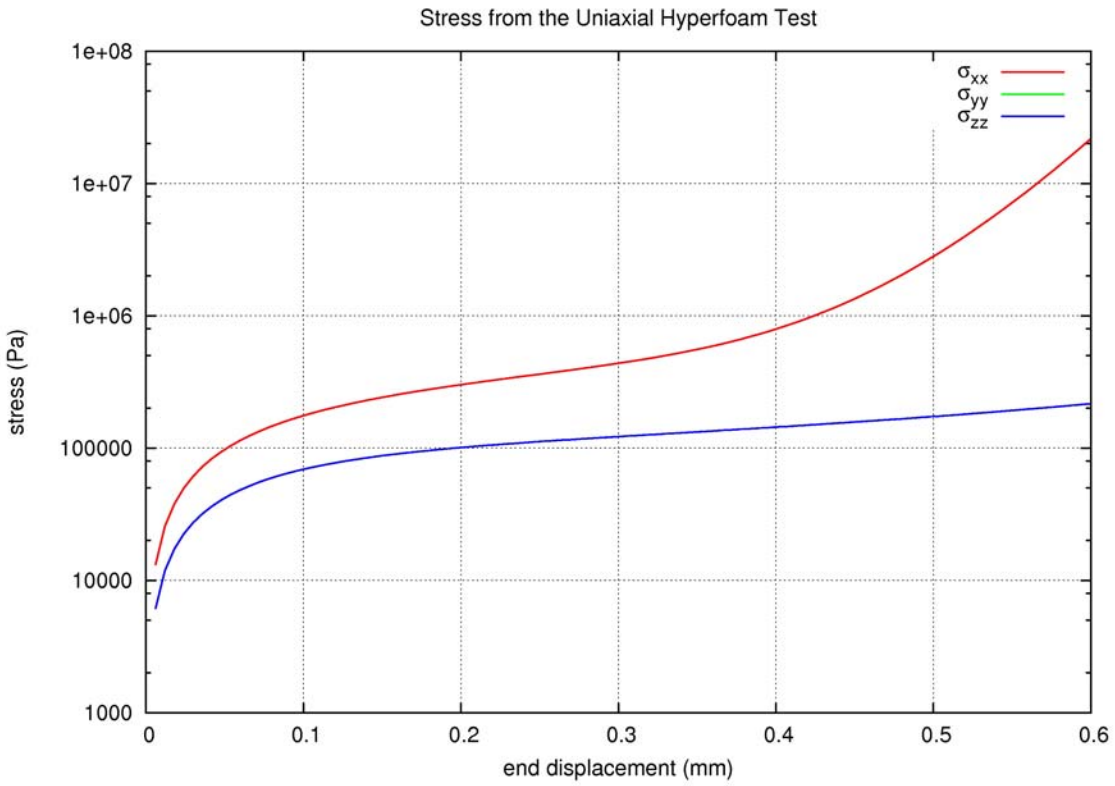

Figure 16: The stress components from the uniaxial hyperfoam test. The principal stresses are oriented along the coordinate directions: $\sigma_1 = \sigma_{xx}$, $\sigma_2 = \sigma_{yy}$ and $\sigma_3 = \sigma_{zz}$.

$$\sigma_1 = \sigma_2 = \frac{1}{\lambda^2}\sum_{k=1}^{3}\frac{2\mu_k}{\alpha_k}\left(\lambda^{\alpha_k} - \lambda^{-2\alpha_k\beta_k}\right)$$
$$\sigma_3 = \frac{1}{\lambda^2}\sum_{k=1}^{3}\frac{2\mu_k}{\alpha_k}\left(1 - \lambda^{-2\alpha_k\beta_k}\right) \quad . \tag{27}$$

3.9.1 Results for Hyperfoam Test

Given the material properties in Table 16, the principal Cauchy stresses can easily be computed for both problems using (26) and (27). The numerical results are shown in Figure 16 and Figure 17. In both cases the principal axes are aligned with the coordinate axes. The numerical results match the analytical results exactly.

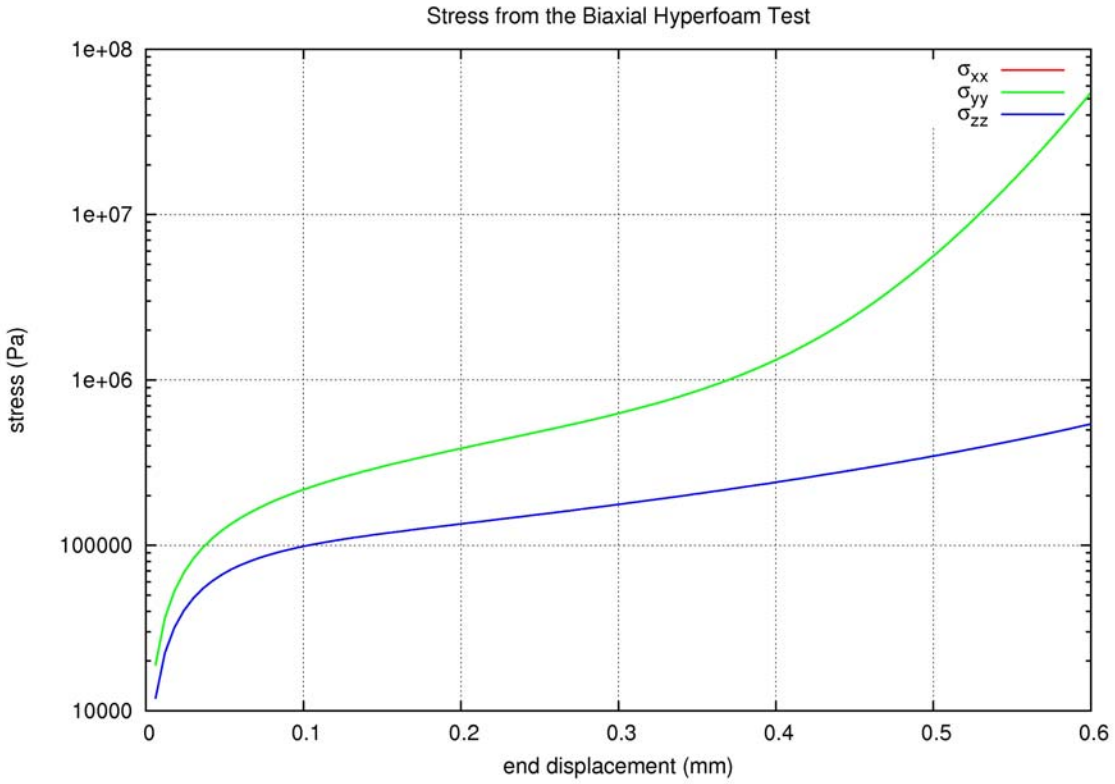

Figure 17: The stress components from the biaxial hyperfoam test. The principal stresses are oriented along the coordinate directions: $\sigma_1 = \sigma_{xx}$, $\sigma_2 = \sigma_{yy}$ and $\sigma_3 = \sigma_{zz}$.

3.10 Low Density Foam Test

The low density foam test is a uniaxial stress problem. The axial loading is displacement controlled with traction free lateral surfaces. The mesh for the problem is the patch-test mesh in Figure 1.

The constitutive model is documented in [11]. The yield function for this model has the form

$$\bar{\sigma} = A\left\langle I_2' \right\rangle + B\left(1 + CI_1\right) , \tag{28}$$

where A, B and C are material properties, $\langle \bullet \rangle$ denotes the Heaviside step function, I_2' is the second invariant of the deviatoric strain and I_1 is the first invariant of the strain.

Table 17. Material properties for the low density foam test

property	value
YOUNGS MODULUS	3010 psi
POISSONS RATIO	0.0
A	49.2 psi
B	60.8 psi
C	-0.517
NAIR	1.0
P0	14.7 psi
PHI	0.090

The test problem is uniaxial compression of the material. The axial compression has a final stretch ratio of $\lambda = 0.25$. Since the problem is traction free for the lateral surfaces, the lateral displacements (strains) are solved for in Adagio. The model will exhibit a slight Poisson effect, but for all practical purposes it can be assumed to have a Poisson's ratio of 0.0.

If the lateral strains are assumed to be zero, the yield function for the solid phase in (28) can be evaluated as

$$\bar{\sigma} = A + B\left[1 + C\left(\lambda - 1\right)\right] . \tag{29}$$

For the input in Table 17 the yield function evaluated at the beginning of the problem is 100 psi and at the end of the problem is about 134 psi. Of course in this analysis the effect of the air is not taken into account. Assuming no lateral strains, this will be about 69 psi. Adding this to the structural stress we will have a stress of approximately 203 psi.

3.10.1 Results for Low Density Foam Test

The results for the compressive stress versus the end displacement (both shown as positive) are in Figure 18. The assumption of zero lateral strains is just an assumption; there will be some lateral strain. From Adagio the lateral displacements are 0.02136 in. The lateral stretch ratios are 1.02136 and the lateral strains are 0.02114. With these values the structural yield stress is 133.24 psi. The pressure due to the air will contribute 63.62 psi so that the final axial stress will be 196.86 psi. This is exactly what the test problem gives for the axial stress shown in Figure 18.

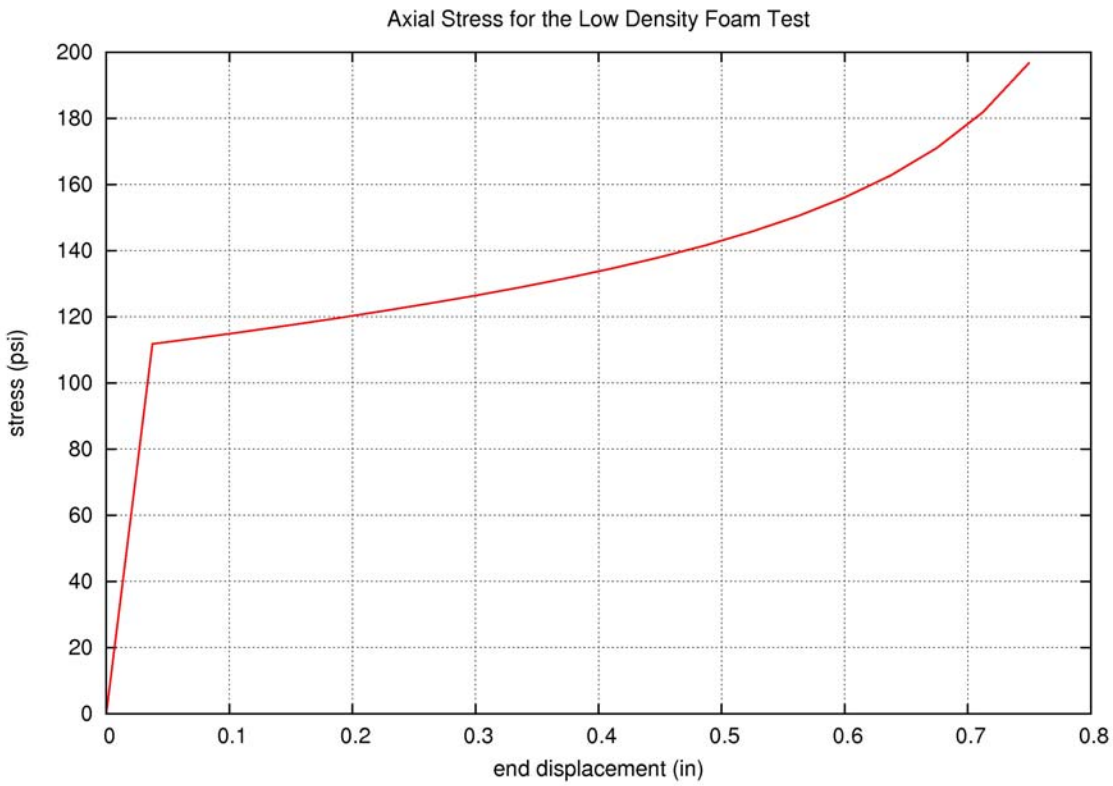

Figure 18: Axial stress for the low density foam test.

3.11 Orthotropic Crush Test

The orthotropic crush model is used to model energy absorbing materials – mainly aluminum honeycomb. This model is one of three models that can be used to model honeycomb; the other two are the orthotropic rate model and the honeycomb model. This model is the simplest one of the three.

Table 18. Material properties for the orthotropic crush test

property	value
YOUNGS MODULUS	1.0×10^{6}
POISSONS RATIO	0.25
YIELD STRESS	2.0×10^{3}
EX	5.0×10^{4}
EY	2.2×10^{5}
EZ	1.0×10^{4}
GXY	1.1×10^{5}
GYZ	5.0×10^{3}
GZX	2.5×10^{4}
VMIN	0.70

The test for the orthotropic crush model is a displacement control, uniaxial stress test. The material is compressed in the *x* direction and is traction free in the *y* and *z* directions. The mesh that is used for the problem is the patch test mesh shown in Figure 1.

The material properties for the model are given in Table 18. It should be noted that the orthotropic behavior of this model is strictly limited to the global axes. In practice this limits the ability of this model to model honeycomb in an actual system. Six crush strength functions are also defined that give the crush strength for the six stress components. As with the material properties, the strengths refer to the strength in the global coordinate system. Plots of the strength curves are shown in Figure 19.

In the regression test, the unit cube is compressed well past the lock-up strain – the volumetric strain where the material strength increases dramatically. For the early stage of deformation the response is elastic with a slope of $E_x = 5\times10^4$ psi. Once the plateau stress is reached, the stress follows the function that defines the crush strength for the *xx* component of the stress. In this case the plateau stress is 600 psi. Finally, at the lock up strain the material behaves as a perfectly plastic material with a yield stress of 2,000 psi.

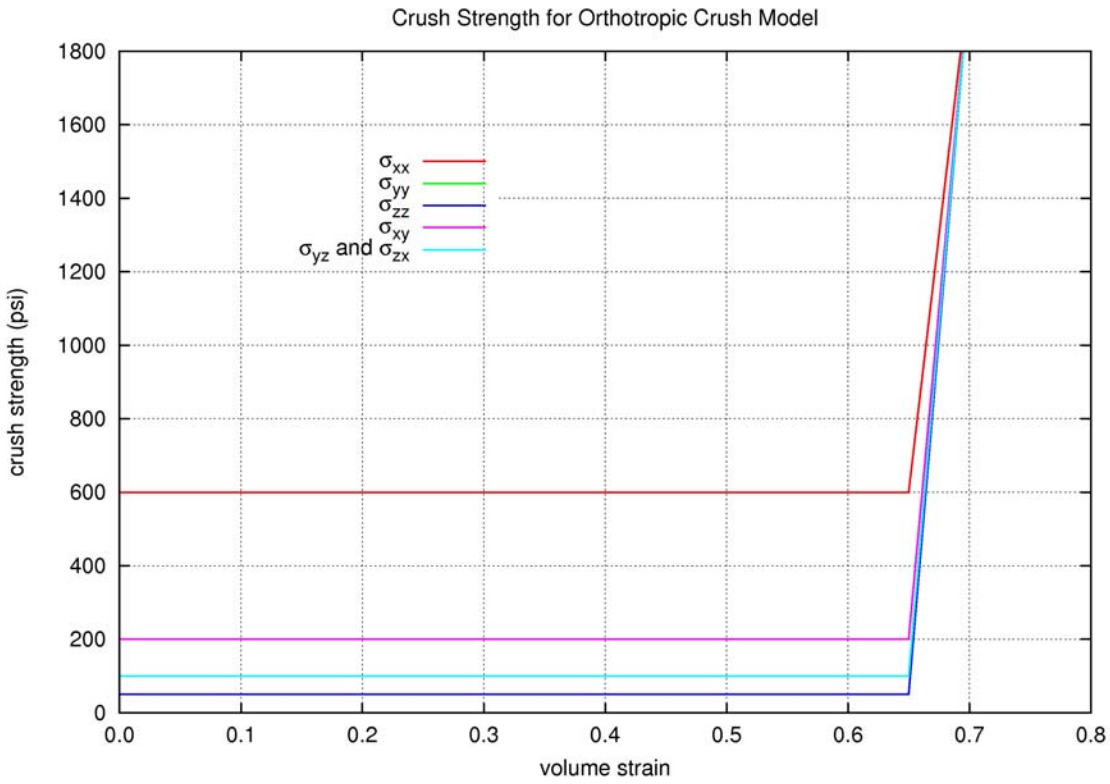

Figure 19: Input crush strength curves for the orthotropic crush test.

3.11.1 Results for Orthotropic Crush Test

The results for the orthotropic crush test are shown in Figure 20. These results match exactly the expected behavior for the model. The initial slope is equal to E_x and the plateau stress of 600 psi is easily seen. The material approaches full compaction at a volumetric strain of 0.65 and reaches full compaction at a volumetric strain of 0.70.

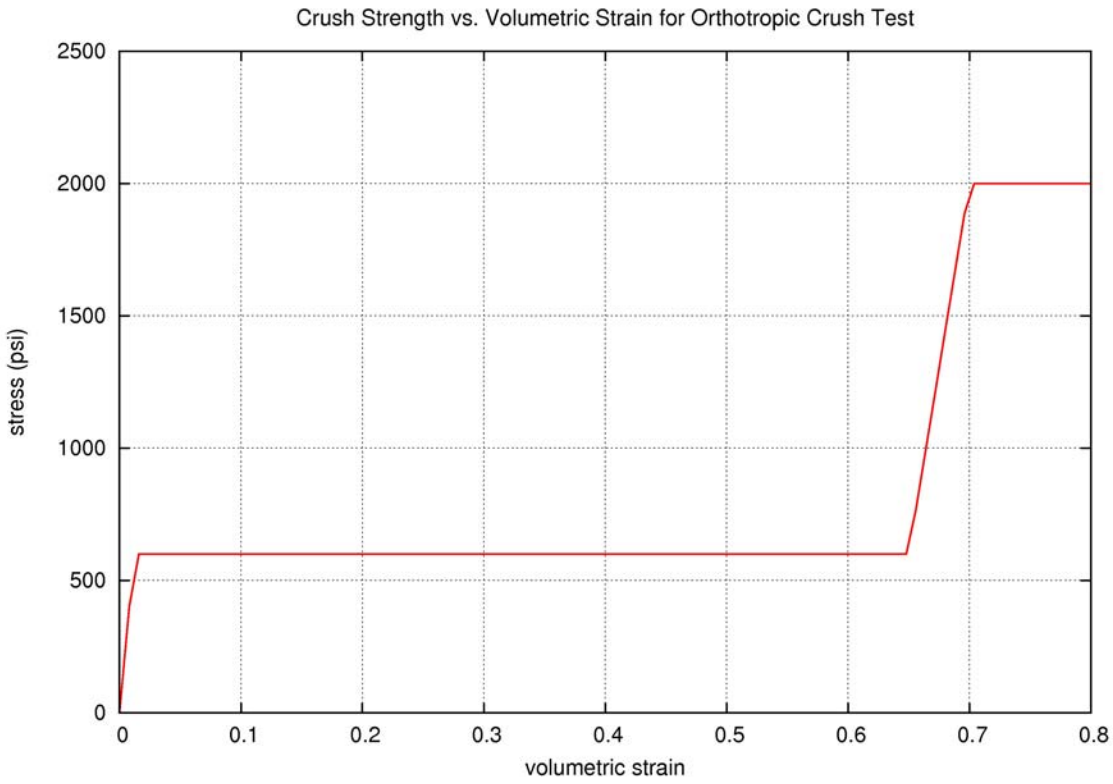

Figure 20: Crush strength versus volumetric strain for the orthotropic crush test.

4. CONCLUSIONS

A number of test problems have been presented that are used as regression tests for the constitutive models in LAME. These regression tests are run in Adagio, a quasistatic solid mechanics code developed on the Sierra framework. The test problems serve three purposes. First, they provide confidence for the constitutive model developer that the model has been implemented correctly. Second, since the regression tests are run on a nightly basis, the problems ensure that the models continue to give the correct answers as code development progresses. Finally, the test problems provide examples for analysts that would like to see what kind of behavior is expected from a particular model.

The tests presented in this report do an adequate job of all three of these functions even though they certainly could be improved or expanded. Other models that are in LAME can be added to the test suite, and many test problems exist that do not appear in this report. However, the job of improving or expanding tests, and especially formally documenting tests, is a long process. Furthermore, the added benefit of creating and documenting more tests, while certainly present, must be weighed against other pressing needs. Over 80 tests currently exist in the test suite, and many have informal documentation that is contained in the test directory. Upgrading the documentation for these tests will always be an on-going effort.

In the future it is expected that this report will grow as more tests are added to the regression test suite and more models are added to LAME. However, concerning testing, no requirements are going to be set upon either the code development teams or constitutive model developers. We hope that the process of developing tests and providing documentation – at least some brief form of documentation, but possibly something more formal – for the constitutive model developer will become a natural part of the model development/implementation process.

5. REFERENCES

1. Scherzinger, W.M. and Hammerand, D.C., *Constitutive Models in LAME*, SAND07-XXXX, Sandia National Laboratories, Albuquerque, NM, XXXX 2007.
2. Scherzinger, W.M. and Hammerand, D.C., *Library of Advanced Materials for Engineering – LAME*, SAND07-5515, Sandia National Laboratories, Albuquerque, NM, September, 2007.
3. Pierson, K.H. and Hales, J.D., 'ADAGIO/ANDANTE User's Guide Version 2.0', Memo, Sandia National Laboratories, Albuquerque, NM, September 2004.
4. Koteras, J.R., Gullerud, A.S., Crane, N.K., and Hales, J.D., *Presto User's Guide Version 2.6*, SAND2006-6093, Sandia National Laboratories, Albuquerque, NM, October 2006.
5. Stone, C. M., *SANTOS – A Two-Dimensional Finite Element Program for the Quasistatic, Large Deformation, Inelastic Response of Solids*, SAND90-0543, Sandia National Laboratories, Albuquerque, NM, July 1997.
6. Taylor, L. M. and D. P. Flanagan, PRONTO3D A Three-Dimensional Transient Solid Dynamics Program, SAND87-1912, Sandia National Laboratories, Albuquerque, NM, March 1989.
7. Stone, C. M., G. W. Wellman and R. D. Krieg, *A Vectorized Elastic/Plastic Power Law Hardening Material Model Including Lüders Strain*, SAND90-0153, Sandia National Laboratories, Albuquerque, NM, March 1990.
8. Krieg, R. D., A Simple Constitutive Description for Cellular Concrete, SC-DR-72-0883, Sandia National Laboratories, Albuquerque, NM, March 1972.
9. Simo, J. C. and T. J. R. Hughes, *Computational Inelasticity*, Springer, New York, 1998.
10. Ogden, R. W., *Non-Linear Elastic Deformations*, Dover, Mineola, NY, 1997.
11. Neilsen, M. K., H. S. Morgan and R. D. Krieg, *A Phenomenological Constitutive Model for Low Density Polyurethane Foams*, SAND86-2927, Sandia National Laboratories, Albuquerque, NM, April 1987.

Distribution

1	MS0346	Tom Baca	1523
1	MS0372	Lupe Arguello	1525
1	MS0372	Joe Bishop	1525
1	MS0372	Robert Chambers	1524
3	MS0372	Daniel Hammerand	1524
1	MS0372	John Pott	1524
1	MS0372	Jim Redmond	1525
3	MS0372	William Scherzinger	1524
1	MS0372	Mike Stone	1525
1	MS0372	Leah Tuttle	1524
1	MS0372	Gerald Wellman	1525
1	MS0380	Manoj Bhardwaj	1542
1	MS0380	Nathan Crane	1542
1	MS0380	Arne Gullerud	1542
1	MS0380	Jason Hales	1542
1	MS0380	Martin Heinstein	1542
1	MS0380	Joe Jung	1542
1	MS0380	Richard Koteras	1542
1	MS0380	Hal Morgan	1540
1	MS0380	Kendall Pierson	1542
1	MS0380	Vicki Porter	1542
1	MS0380	Garth Reese	1542
1	MS0380	Ben Spencer	1542
1	MS0380	Tim Walsh	1542
1	MS0384	Arthur Ratzel	1500
1	MS0555	Rod May	1522
1	MS0557	Dave Clauss	1521
1	MS0660	Chris Lamb	9512
1	MS0836	Shane Schumacher	1516
1	MS0847	Mike Neilsen	1526
1	MS0847	Pete Wilson	1520
1	MS1070	Channy Wong	1526
2	MS9018	Central Technical Files	8945-1
2	MS0899	Technical Library	4536